Research Journal of Chemical and Environmental Sciences
Res J. Chem. Environ. Sci. Vol 7 [3] June 2019: 35-51
Online ISSN 2321-1040
CODEN: RJCEA2 [USA]

Website: www.aelsindia.com/rjces.htm

RJCES

ORIGINAL ARTICLE

Climate variability and hydrogeological responses in the mountainous area of Ennedi (Chad) using remote sensing

[1]Miradj Habib Djafar, [1]Abderamane Hamit and [2]Marie-louise vogt
[1]Department of Geology, Faculty of Exact and Applied Sciences, University of N'Djaména, Chad
[2]Centre d'Hydrogéologie et Géothermie, University of Neuchâtel, Neuchâtel, Switzerland

ABSTRACT
Through the study of climate variability and its response on the hydrogeology of the Ennedi area, this research aims to improve knowledge on the functioning of the aquifer system of the Ennedi mountain area with a view to better mobilization and sustainable management of water resources. Ennedi is characterized by an arid to hyperarid climate where the only available water resource is groundwater, which has been greatly weakened by climate change in recent decades. A study using remote sensing was carried out. The result of this study provided a good understanding of the spatial and temporal variability of climate and the relationship between rainwater and groundwater. The rainfall maps highlighted the heterogeneity of the spatial distribution of rainfall and made it possible to locate deficit and surplus areas. Results obtained in this study confirm once again the possibilities offered by Landsat8 OLI/TIRS satellite data to solve the energy balance equation by estimating evapotranspiration. The calculation of the water balance made it possible to quantify the volume of water that will contribute to the recharge of the Paleozoic sandstone aquifer of the Ennedi.
Key words: Ennedi, climate variability, hydrogeological responses, recharge, aquifer, remote sensing

Received 07.04.2019 Accepted 25.05.2019

INTRODUCTION

Located on the northern and eastern borders of Chad, Ennedi is a spacious geomorphological unit that, together with Borku and Tibesti, forms the southern border of the great SAHARA. It contains a huge mountainous massif (which is the mountainous area in question) with impressive natural beauty and biodiversity systems. The Ennedi massif is a succession of sandstones ranging from Cambro-Ordovician to Upper Devonian, resting in discordance on the Precambrian basement and underlying the marine limestone of the Carboniferous age. It is highly fractured and eroded by wind and thermal cycles that have significantly increased its storage capacity and transmissivity[10]. At an altitude of 1,450m, it records increased precipitation due to these increases compared to the surrounding lowlands, thus giving it a favourable climate[18]. Due to its remoteness and uncomfortable climatic conditions, the Ennedi region has still relatively been unexplored. There is very little knowledge about water resources. Ennedi is characterized by an arid to hyperarid climate where the only available water resource is groundwater, which has been greatly weakened by climate change. Recent climate trends show that since 1970 the area has been subject to a 50% decrease in annual rainfall [3]and a temperature increase of 0.8°C [6]compared to the previous period. It is expected that future developments will continue to follow this same trend, putting the resource under pressure with significant consequences. Evaporative events are extremely high compared to rainfall [12]; [3], only part of the precipitation infiltrates, the importance of this infiltration determines the possibilities of groundwater recharge. Quantifying the proportion of precipitation that recharges groundwater and capturing its frequency would go a long way towards improving our knowledge of storage capacity and aquifer dynamics for effective water resource management.This study aims to evaluate the spatial and temporal variation of rainfall in the Ennedi, to see the response of the aquifer system to these variations, and to make a water balance including an estimate of the quantity of water that would contribute to modern groundwater recharge as well as the frequency of this recharge. Test new methodologies to overcome the lack of field information in this region using an innovative approach based on the use of the latest advances in space technology. In particular, the estimation of evapotranspiration from Landsat8 images by the energy balance equation using the S-SEBI approach.

Geographical and Geological Background

The Ennedi region is located in the north-east of Chad between the 15th and 21st degrees of latitude North and the 20th and 24th degrees of longitude East (Fig.1). It is characterized by a Saharan climate, arid in its southern part and hyperarid in its northern part. This character is linked to the annual influence of the monsoon which brings modest rainfall, especially in the southern part of the Ennedi. The region contains several morphological units: the Mourdi depression in the north, the Djourab on the western edge of the massif, the Mortcha plain and the Ennedi massif.The Ennedi massif takes the form of a rectangular triangle with a total estimated surface area of 51,210 km^2[14]. It is bounded to the south by the Precambrian basement of the Ouaddaï and to the north by the Mourdi depression which separates it from the Erdis relief line and the Jef-Jef plateaus constituting the boundary between the Chadian and Libyan basins [18]. To the east, the reliefs of the Erdébé plateau, the eastern end of the massif, are gradually invaded and disappear under the sands of the Sudano-Libyan desert. To the west, the relief of the Ennedi massif fades into the Bir Kora area, while the Precambrian basement and Cambrian-Ordovician sandstones gradually sink deeper.

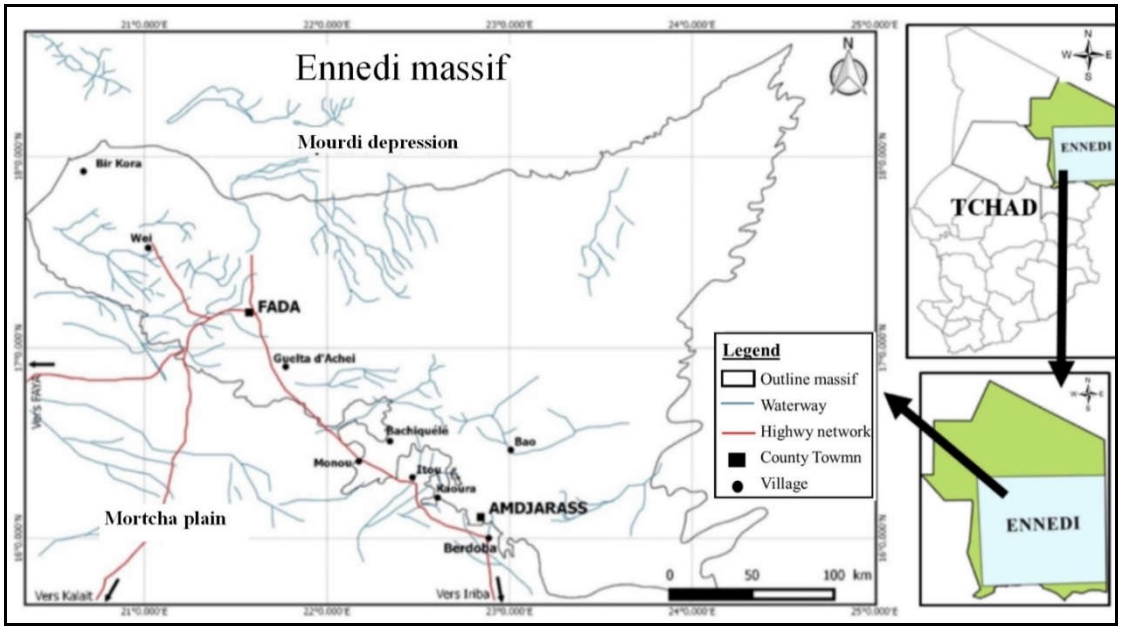

Figure1: Location of the study area

After the Pan-African orogeny (750 MA to 600 MA), an important basin was created at the level of the Ennedi and which was filled from the beginning of the Cambrian by clayey-gravel deposits of continental origin. These sandstone complexes lie in unconformity on the Precambrian basement and overlook the carboniferous formations. The formations often have good permeability related to cracking and fracturing due to tectonic actions [17]. Figure 2 illustrates the different geological units of the area according to Wolf [19].

Data used and methods

The lack of field data has led us to use remote sensing data. Today, with the development of technology, satellites are producing information as quickly as possible. They offer good regularity over time and homogeneity in spatial coverage. The use of satellite data has increased significantly in recent years in multiple research areas: estimation of daily precipitation, estimation of evapotranspiration, determination of NDVI or NDWI.The database consists of three data sets. A first set was created using the RFE2/FEWS-NET images to extract rains at monthly and ten-year time steps for the time series 2000-2016. The second one contains the observed daily evapotranspiration values for each pixel of the LandSat8 OLI/TIRS images over the period 2013 to 2015. And the last one concerns the variation in storage obtained by synthesizing the GRACE data at monthly time steps.

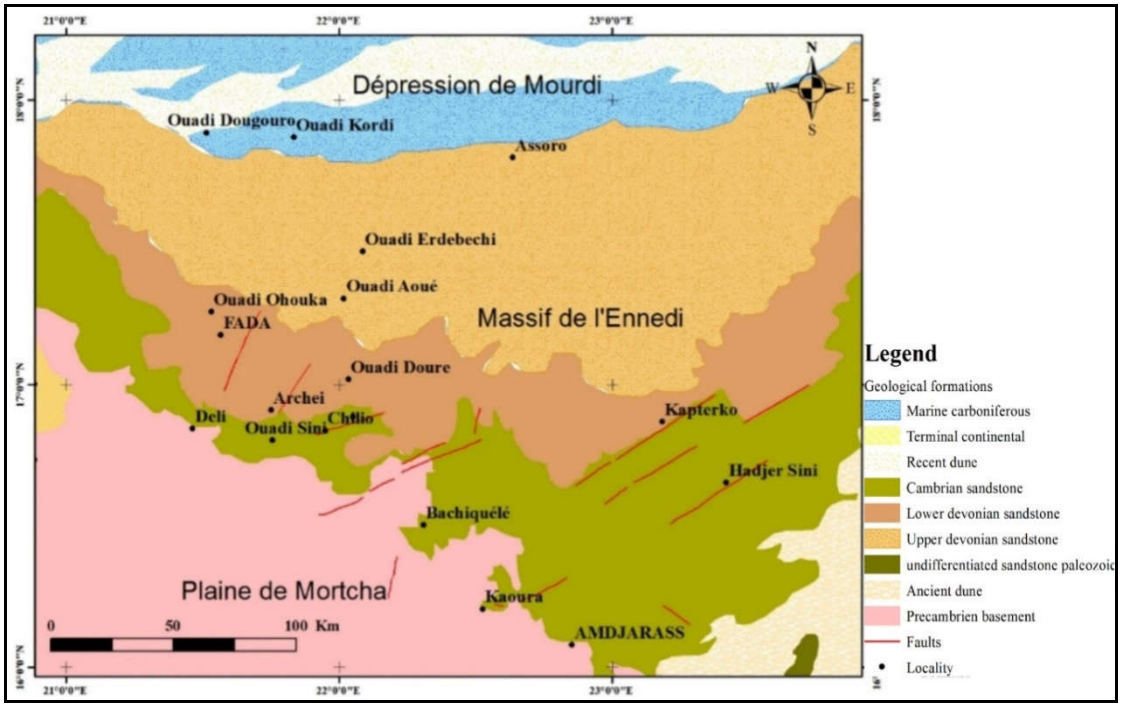

Figure2: Geological map of the study area (Source: Geological map of the Republic of Chad by Wolf [19])

Method for analyzing rainfall variability

Since RFE2 provides quarterly, bimonthly, monthly and decadal data, we have chosen the latter two for this study. The ten-year data were used to calculate the water balance because of their temporal resolution (10 days). The monthly data were used to study rainfall variability. As the rainy season in the Ennedi massif is limited only to July, August and September, the data set used concerns only these three months (from the first decade of July to the last decade of September).

The analysis of rainfall variability by anomaly (relative deviation) made it possible to characterize the rainfall between the inter-annual mean of the series studied and the annual mean totals. The anomaly calculation makes it possible to highlight the surplus and deficit periods within a time series.

$$E = \frac{(P_i - P_{moy})}{P_{moy}} * 100$$

Where

E: Relative deviation or anomaly (%)

P_i: Average annual precipitation recorded during the year i (mm)

P_{moy} = Mean inter-annual precipitation of the series studied.

Method for estimating evapotranspiration

To estimate evapotranspiration, Landsat8 OLI/TIRS images are used. Indeed, they make it possible to detect changes and variations in the presence of water at a scale adapted to the size of the hydrographic network that conserves water for a sufficient time to be captured by the satellite. To cover the study area, three Landsat scenes were required: 81/48, 180/48 and 180/49. From these scenes, we chose a series of images without clouds (0% clouds) but with the presence of surface water accumulations that are used to calculate evapotranspiration. The lack of water in the images results in a cessation of evapotranspiration phenomena. However, the exchange of energy between the ground and the atmosphere continues. On this basis, we used 42 Landsat8 OLI/TIRS satellite images: 14 for 2013, 18 for 2014 and 10 for 2015. Details of all these images are recorded in Table 1.

Tableau1: Description of the images used to calculate evapotranspiration

Path/raw image	2013		2014		2015	
	ID image	Acquisition date	ID image	Acquisition date	ID image	Acquisition date
181/48	234	August 22nd	237	August 25 th	240	August 28 th
181/48	250	September 7th	285	October 12 th	272	September 29 th
181/48	282	October 9 th	301	October 28 th	288	October 15 th
181/48	298	October 25 th	317	November 13 th	304	October 31 st
181/48			333	November 29 th		
180/48	227	August 15 th	214	August 2nd	217	August 5 th
180/48	243	August 31st	230	August 18 th	249	September 6 th
180/48	259	September 16 th	246	September 3 rd	281	October 8 th
180/48	275	Octobrer 2nd	262	September 19 th		
180/48	307	November 3rd	278	October 5 th		
180/48			294	October 21 st		
180/48			310	November 6 th		
180/48			326	November 22nd		
180/49	243	August 31 st	230	August 18 th	217	August 5 th
180/49	307	November 3 rd	246	September 3 rd	249	September 6 th
180/49	323	November19th	278	October 5 th	281	October 8 th
180/49	339	December5th	310	November 6 th		
180/49	355	December 21st	326	November 22nd		

For the determination of evapotranspiration by remote sensing, the latent heat flux (***λE*** which is the equivalent of evapotranspiration) is generally estimated through the resolution of the energy balance equation **[11]**:

$$\lambda E = Rn - G - H$$

λE: the flow of latent heat released by evaporation (W.m-2) ;(W.m-2);
H: the sensible heat flux released into the atmosphere (W.m-2);
Rn: the net radiation at the surface (W.m-2;
G: the heat flux in the ground (W.m-2).

The method used to estimate evapotranspiration is based on the S-SEBI (Simplified Surface Energy Balance Index) approach. This approach uses the correlated relationship between latent heat and sensible heat, which is highly dependent on the water content of the system, to estimate the evaporation fraction**[15]**. The general assumption is that wet surfaces have an evaporation fraction of 100% and completely dry surfaces have an evaporation fraction of 0%. The evaporation fraction, considered stable at a one-day scale **[2]**, is used to allow the passage from an instantaneous magnitude of latent heat flux measured by the satellite to a daily magnitude that corresponds to the actual evapotranspiration **[15]**. The following methodological flowchart (Fig. 3) illustrates the handling procedures.

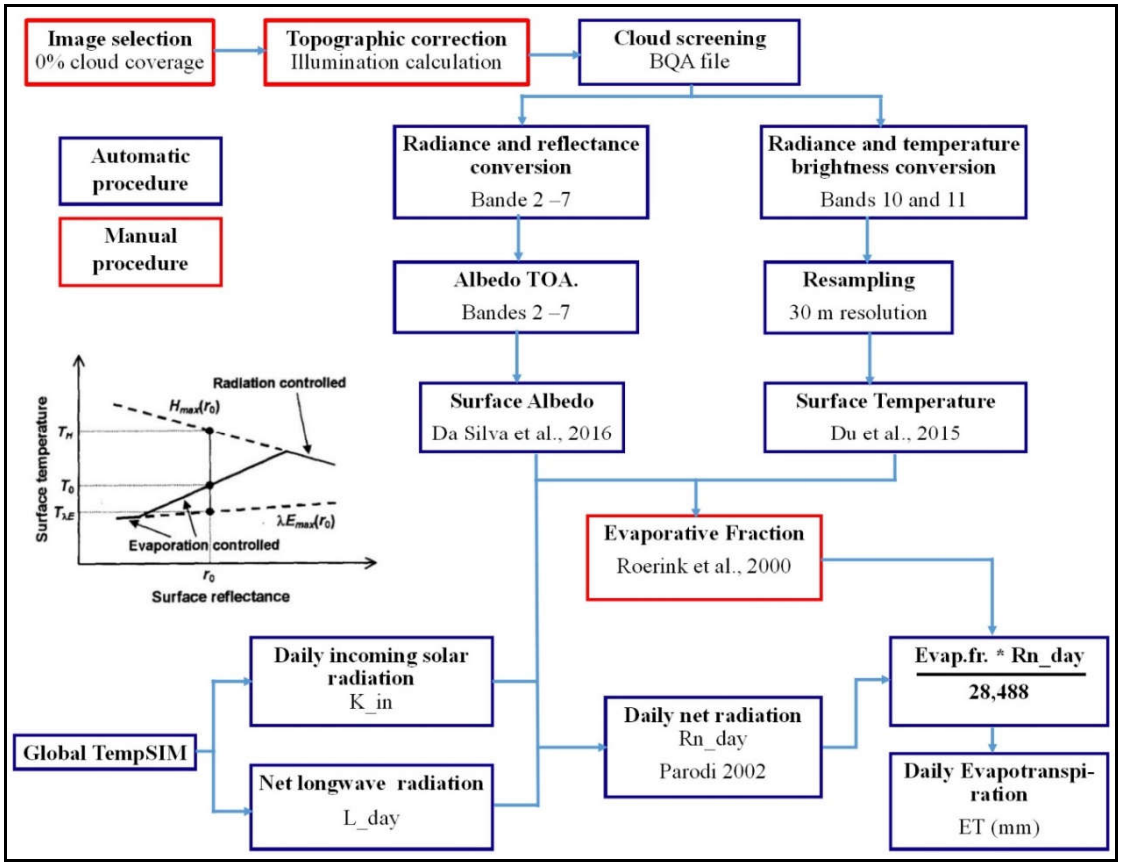

Figure3: Method of calculating evapotranspiration from Landsat8 OLI/TIRS images

The preliminary processing consists in transforming the bands into spectral luminances. An atmospheric correction follows this step to remove shadows that can be confused with water accumulation areas. After this correction, the spectral luminances are converted into radiances and reflectance's and are then used to calculate the surrounding albedo(r) and surface temperature.

- Surrounding albedo ( ) characterizes the fraction of solar radiation falling at the bottom of the atmosphere that is reflected from the surface **[1]**. The procedure used to calculate the albedo is the one proposed by Da Silva and his collaborators**[4]**:

$$r = \frac{(r_{toa} - r_{atm})}{\tau oc^2}$$

r: Surface albedo
r_{toa}: Albedo without atmospheric correction (without unit)
r_{atm}: Atmospheric albedo = 0.03
τ_{oc}^2: Atmospheric transmittance in the solar radiation domain = 0.5

- The surface temperature was calculated using the method of Du and his collaborators**[5]**according to the formula:

$$T_C = T_k - 273.15$$

With

$$T_k = \frac{-2.78009 + 1.0151 * (b10_T + b11_T)}{2 + 4.9292 * (b10_T - b11_T)} \\ 2 + 0.09152 * ((b10_T - b11_T)^2)$$

Where

$T_{C\ :Surface}$ temperature in degrees Celsius
T_k : Surface temperature in Kelvin
$b10_T$ and $b11_T$: the temperatures (in Kelvin) of bands 10 and 11 respectively;

- The evaporation fraction ***(EF)*** is the energy partition between the different components of the energy balance. It is calculated according to the S-SEBI [15]. It is expressed as a function of surface temperature (T_C), albedo (r) and variables **a, b, c** and **d** which are manually determined using the

properties of wet/dry pixels and surface water conditions from the graph relating reflectance and surface temperature (fig. 3).

$$FE = \frac{b + (a * r) - T_c}{b - d + (a - c) * r}$$

Evapotranspiration can be defined as the amount of water that is dissipated into the atmosphere by the vaporization process. Daily evapotranspiration is obtained by combining the daily net radiation and the evaporation fraction. We thus move from an instantaneous quantity to a daily quantity. Parodi method was used to express actual daily evapotranspiration (***AET***)[13].

$$ETR = \frac{FE * R_n}{28.588}$$

With R_n the daily net radiation (W m-2)

Calculation of the water balance

We considered a water balance whose general assumption is that all waters that precipitate within the watersheds converge towards the rivers. Some of this water evaporates and some infiltrates (considered here as the amount of water that contributes to the recharge). The balance is characterized by the only input, which is the contribution of precipitation, and the only output, which is evapotranspiration. The difference between these two components is therefore the residual meaning the quantity of water involved in the recharge. Underground flows and contributions from adjacent basins are excluded and are not included in this exercise. The water balance is established according to the following general equation:

P - ETR = +R+I

With:
P: Precipitation (in mm);
AET: Actual evapotranspiration (in mm).
R Run-off (mm)
I: Infiltration (mm)
Where R+I is the effective rain that contributes to recharging.

RESULT AND DISCUSSION

Annual rainfall variability from RFE2/FEWS-NET

The distribution of rainfall from RFE2/FEWS-NET is very irregular. This irregularity shows that the region is subject to particular meteorological phenomena that do not follow a single trend. Rainfall is generally less than 100 mm/year with a high inter annual variability, typical of an arid climate. The wettest year is 2010 with a total of 113 mm and the driest year is 2004 with a total of 24 mm (Fig. 14). It can be seen that at the series level, each wet year is followed by a less humid year than it is. And, when two less humid years follow one another, the following year will be particularly humid (example of the year 2010). This same observation was observed from 2014 onwards, when there was a decrease in the annual totals for 2015 and 2016. If the evolution follows the trend explained, it is expected that 2017 would be wetter than 2015 and 2016. The inter annual average of the series is 61mm. Note that RFE2/FEWS-NET overestimates precipitation estimates, however, it is important not to lose sight of the errors that these values may have.

The coefficient of variation (defined as the ratio between the anomaly and the inter annual mean) is slightly high (0.42), therefore the dispersion of the annual mean rainfall amounts around the inter annual mean has varied considerably.

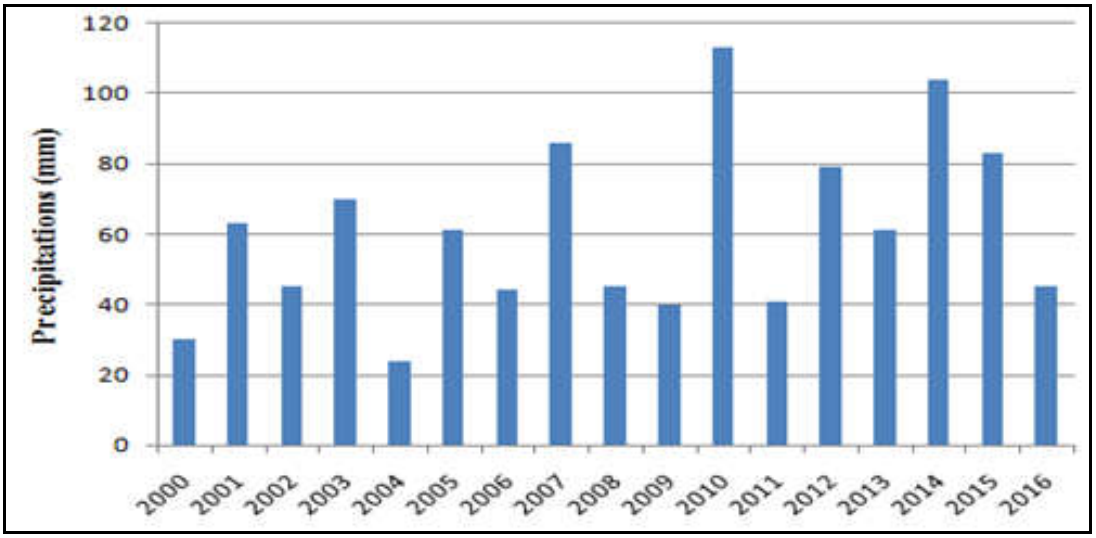

Figure4:Histogram of average annual precipitation from 2000 to 2016 calculated from RFE2/FEWS-NET

The analysis of rainfall variability by the anomaly test (relative deviation) made it possible to distinguish two climatic periods (Fig. 5). A period of poor rainfall (2000 - 2009) characterized by a dry climate and a surplus period (2010 - 2016) where the climate is humid.

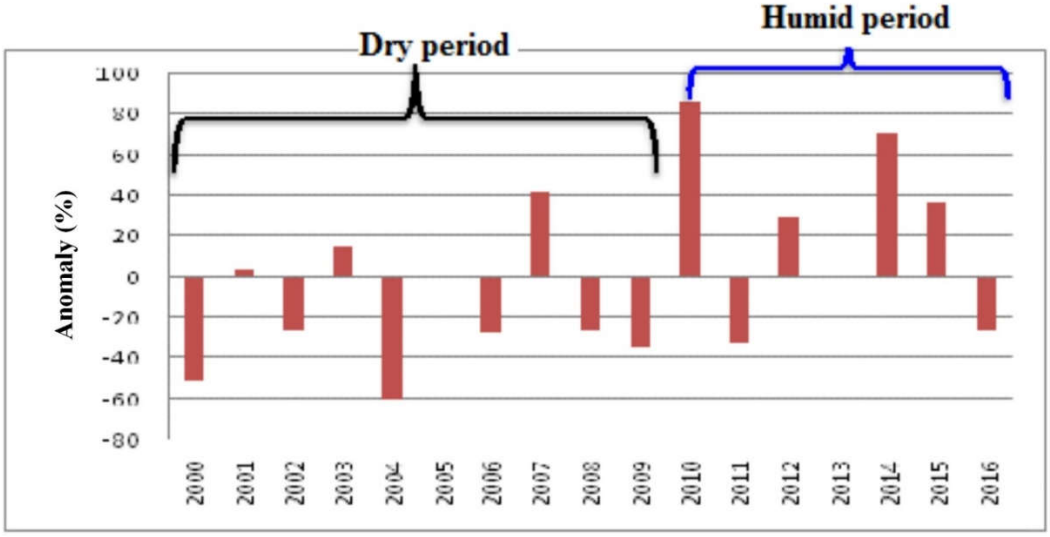

Figure5: Histogram of the rainfall anomaly

The observation of the rainfall distribution histogram (Fig. 6), showing the rainfall amounts for the two periods, shows a shift to the right of the graph for the rains from 2010 to 2016 compared to the decade 2000-2009. This shift is explained by an increase in precipitation for this period. Although there is a very high variability that is difficult to identify, a rainfall deficit can be observed over the dry period. The annual average for this period is 51 mm. From 2010 onwards, there is a recovery in good rainfall, annual totals of over 100 mm (2010 and 2014) have been recorded and the annual average rainfall is 75 mm, an increase of 24 mm on average.

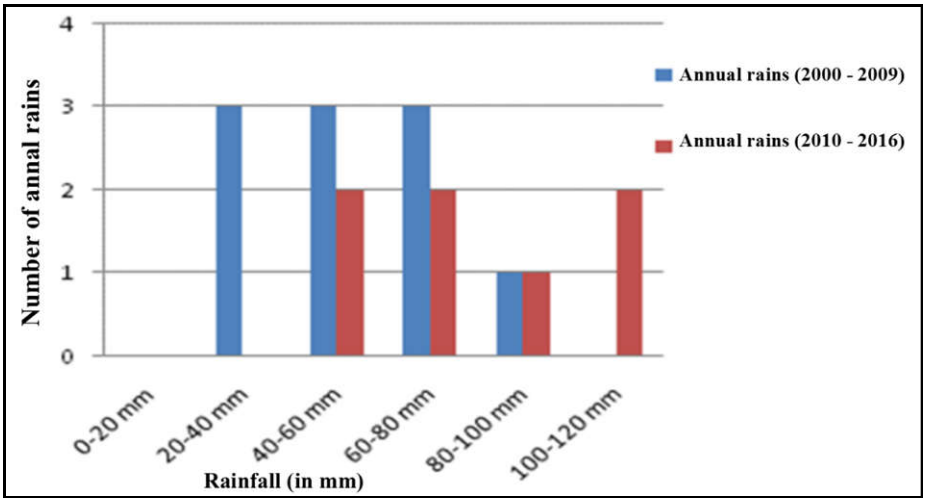

Figure6: Rainfall distribution histogram

Annual precipitation mapping

The annual precipitation mapping reflects the spatial evolution of rainfall variability while highlighting deficit and surplus areas. There are four well-defined climate zones: The spatial distribution of precipitation is heterogeneous throughout the study area. Rainfall variability, strongly influenced by climate change in recent decades, reflects the great heterogeneity in the spatial and temporal distribution of rainfall during this period. The analysis in Figure 7 shows a clear incurvation of isohyets marked by a gradient that gradually and steadily decreases in a southwest to northeast direction: mean annual rainfall totals range from over 100 mm in the extreme southwest to values below 20 mm in the Mourdi depression. There are four well-defined climate zones:

- The extreme southwest at the level of the Mortcha plain and part of the southern edge of the massif (Bachiquélé) which are the most watered receive more than 100 mm of rainfall;
- The southern edge of the massif, at the foothills of the Fada and Archei line, which lies between the 100 and 50 mm isohyet;
- The high plains, at Bao, Moutougouni and the northern edge of the massif where the annual rainfall is between 20 and 50 mm;
- The northern part of the Mourdi slope north of the 20 mm isohyet corresponds to the hyperarid zone.

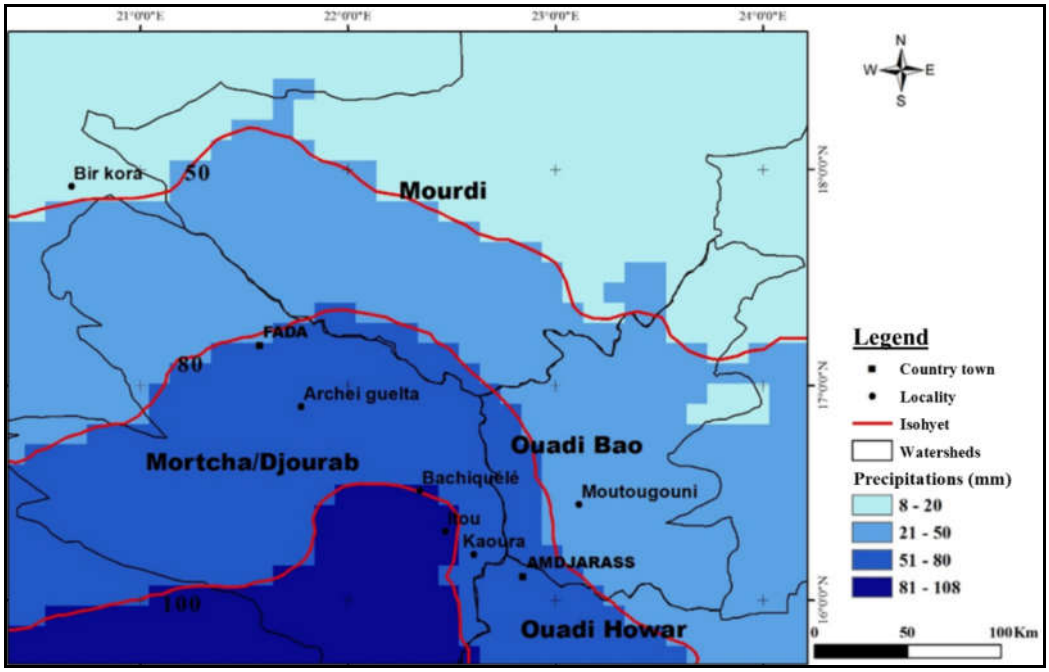

Figure7: Spatial variation of precipitation from 2000 to 2016

Precipitation mapping for both periods (surplus and deficit)

By referring to the calculation of anomalies, a distinction is made between the deficit period and the surplus period. The cartographic representation of precipitation for these two periods varies significantly from one period to another. The interpretation of Figure 17 shows that:

- During the 2000 - 2009 period, the northern part of the area (from the Mourdi basin divide and the Mortcha/Djourab divide) and the northeastern part of the Bao basin, which occupy half of the area, received rainfall of less than 20 mm/year. A reduction in rainfall is also observed in Fada, Archei and Amdjarass, which have rains of between 20 and 50 mm/year. In short, there is a reduction in the rainfall field compared to the interannual average resulting in a sliding of isohyets. Isohyet 80 slides southwest and gives way to isohyet 50;
- The 2010 - 2016 period is characterized by a recovery in rainfall, which generally waters the entire area. This increase is marked by the migration of isohyets. The isohyet of 20, which covers half of the area in the previous period, migrates to the Northeast and shrinks to a small part. On the southern edge of the massif, there is an increase in rainfall of more than 100 mm/year, a fact not observed during the previous period.

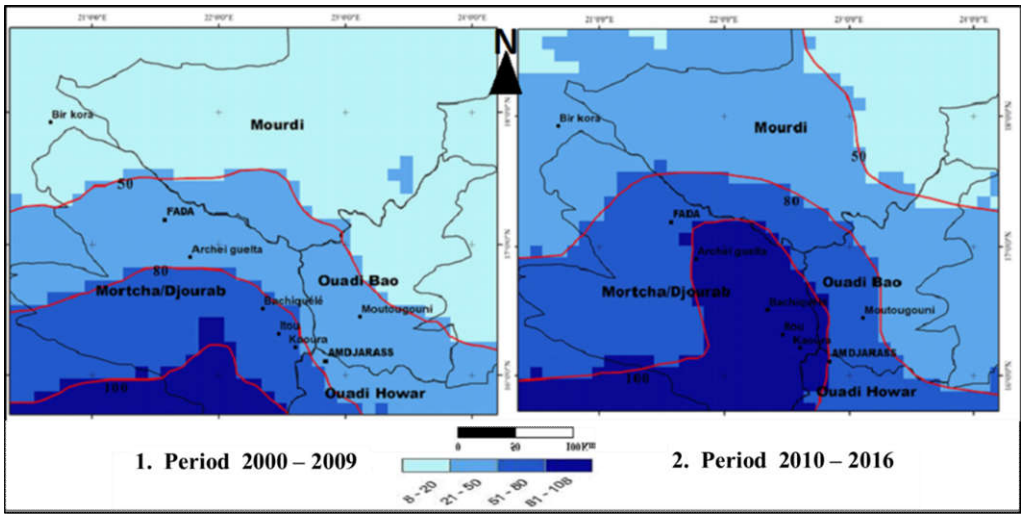

Figure8: Spatial variability of rainfall in both periods (deficit and surplus)

Contribution of remote sensing to evapotranspiration estimation

Given the complexity of the handling techniques and the enormous time required for processing, the study focused on the years 2013 to 2015 to estimate evapotranspiration. The variables required to estimate the evapotranspiration obtained are: surface temperature, albedo, net radiation and evaporation fraction.

Surface temperature

The values obtained for the surface temperature are speckled with errors for some images. It was necessary to correct the data before it was used. For all images, the surface temperature varies between 10.2ºC corresponding to the minimum value of day 355 and 58.8ºC corresponding to the maximum value of day 259. This spatio-temporal variability of temperature highlights the particularity of the landscape characterized by bare ground occupying most of the area, which thus causes an advection phenomenon resulting in an increase in the evapotranspiration process. The higher temperature values generally correspond to surfaces where bare soils are dominant, while the lower values are due to very recurrent humidity in some areas of the wadis where there is water accumulation and/or dense vegetation cover all around (Fig.9).

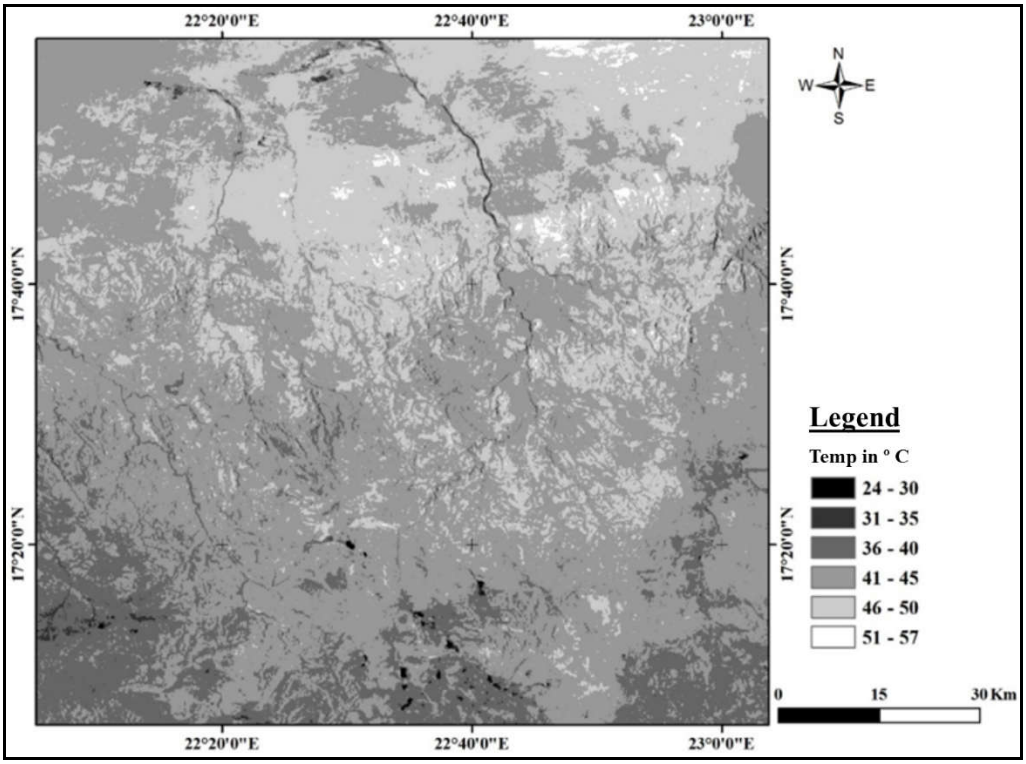

Figure9: Corresponding surface temperature on day 230 of 2014

Surface albedo

Albedo expresses the ratio between the energy of electromagnetic waves reflected by a surface, by reflection or scattering and the energy of incident electromagnetic waves. The values obtained range from 0.02 to 0.95. Albedo is very high in bare soils covered with very light sands that over-reflect radiation. It is a little low for the dark body, as in the case of rock formations, as shown in Figure 10. The surface albedo does not vary too much from one image to another.

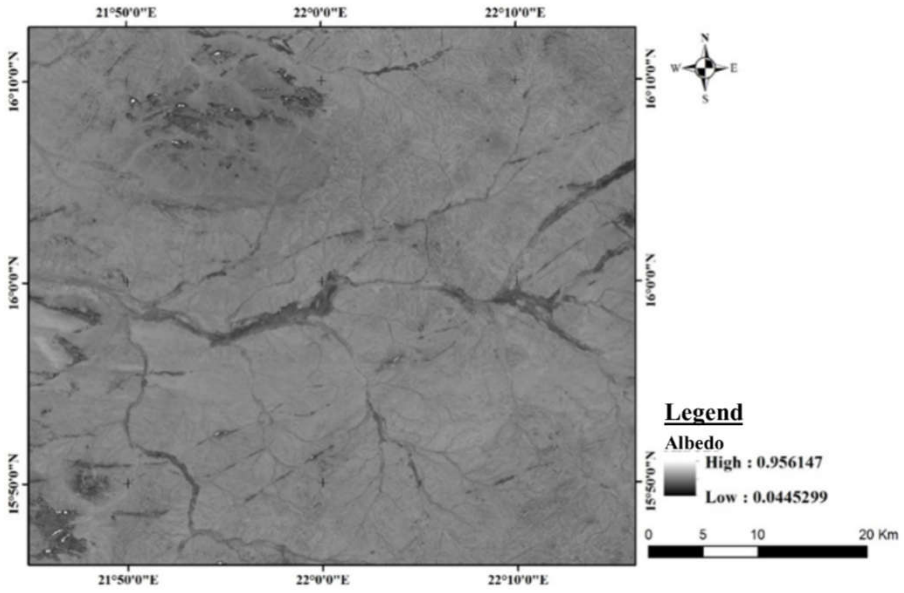

Figure10: Variation of the surface albedo

Net radiation

The net radiation values obtained from the images range from 3.7 W/m^2 to 225.7 W/m^2. Wet river beds and surface water accumulation areas are represented by high values. Bare soils are characterized by low values (Fig. 11).

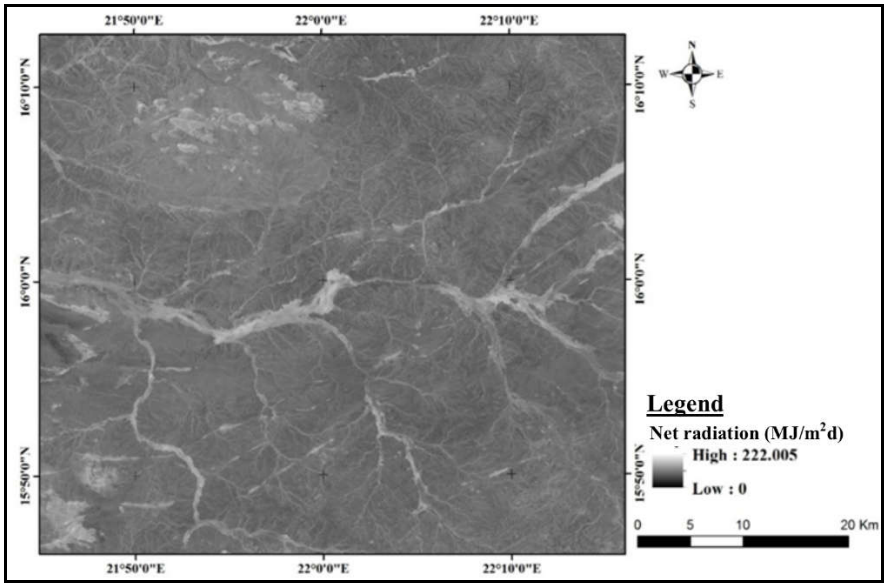

Figure11: Distribution of net radiation

Actual Evapotranspiration (AET)

Actual evapotranspiration is a major component of the water balance. It expresses the mass and energy exchanges between the soil-water system and the atmosphere. The latent heat flux λE, which represents the energy equivalent of evapotranspiration, has been estimated by remote sensing methods that are essential tools for evaluating evapotranspiration both in space and time. Values range from 0 to 7.9 mm evapotranspiration per day. They seem to have some consistency despite the uncertainties. High evapotranspiration values are observed over areas of surface water accumulation and in wet beds of wadis where albedo is low (Fig. 12). Bare soils covered with sands that have a very high albedo have low evapotranspiration values.

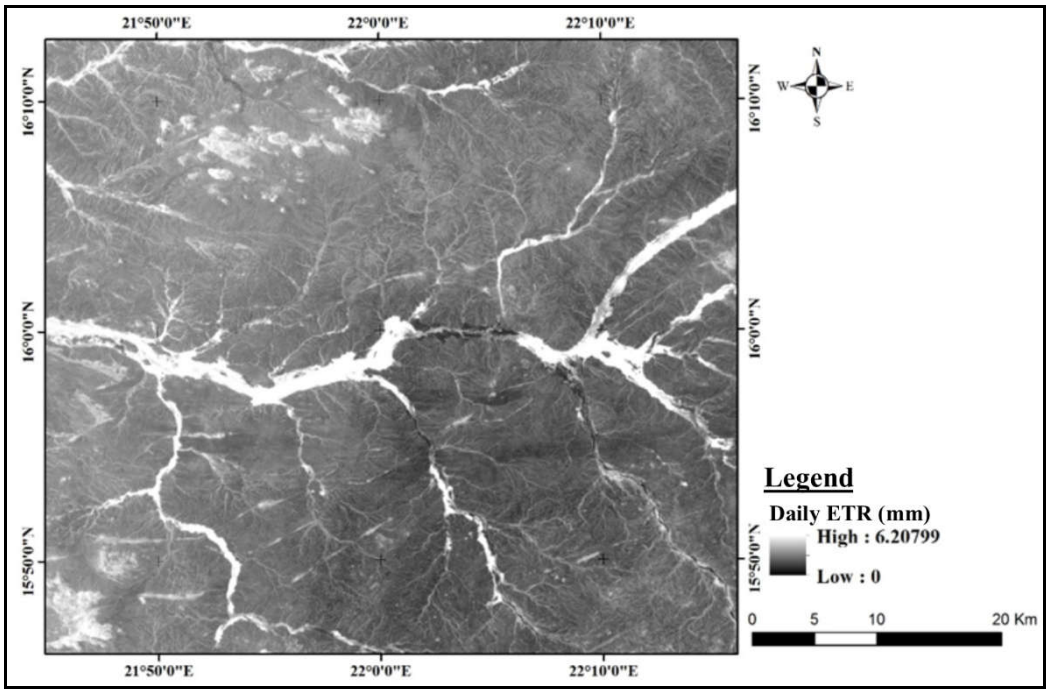

Figure12: Example of the distribution of evapotranspiration

Variation in groundwater storage

With GRACE, it is now possible to track the interannual variation of groundwater storage. The test done in this study revealed the strong annual and interannual variations (Fig. 13). Since the variations in the gravity field related to rock masses do not change annually, it is certain that these variations are due to water storage which varies not only annually but also month after month. And as in the region, there is no other source of water that feeds groundwater tables except rainwater, it can be said that rainwater is responsible for these variations. Coupled with precipitation data, GRACE data show some correlation (Fig. 14). We can see that the change in storage is very sensitive to rainfall variations. As the rainy season approaches, the variations are so small that they are close to zero, which supports our assumption that the storage variation is considered to be zero. A slight increase was observed at the end of July in response to the rains that fall to recharge the aquifer system. This increase continues until the end of the rainy season before relapsing.

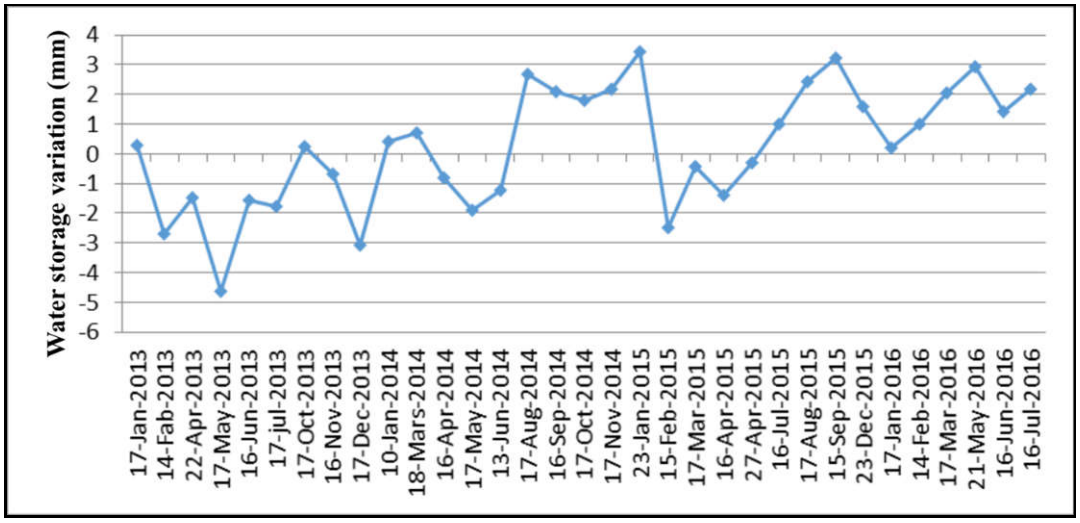

Figure13: Storage variation between 2013 and 2016

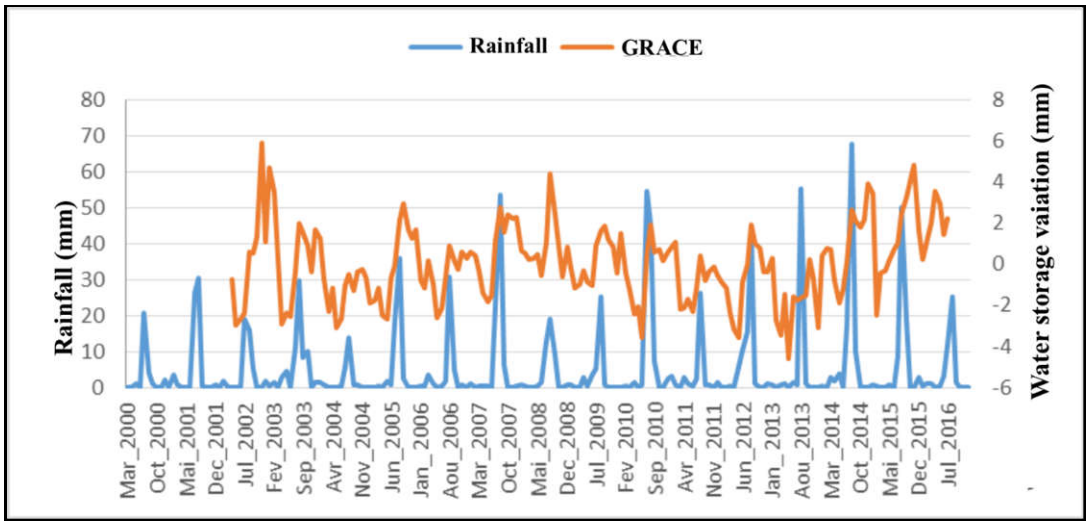

Figure14: Correlation between GRACE data and rainfall data

Water balances

The calculation of the water balance is the most commonly used method for estimating recharge [8]. It is also an important tool for better understanding certain issues related to water in arid zones. It therefore makes it possible to highlight the evolution of effective rainfall given by the difference between rainfall inputs and evapotranspiration losses. If we consider a water balance at annual time steps, we will obviously have a deficit balance because annual evapotranspiration is much higher than annual precipitation in any given year. Hence the interest of carrying out a monthly study that only concerns the rainy season (July, August and September) since it is in these months that the rains are recorded. We have

therefore calculated water balances for three consecutive years (2013, 2014 and 2015) to quantify the proportion of precipitation that escapes evapotranspiration and reaches aquifers to recharge groundwater (Table 2).

Table2:Summary of water balance results

	2013			2014			2015		
Days	**P** (mm)	**ETR** (mm	**R** (mm)	**P** (mm)	**ETR** (mm	**R** (mm)	**P** (mm)	**ETR** (mm)	**R** (mm)
20-31 Jul				23.1	14.9	8.2			
1-10 Aug				36.1	14.1	30.2	21.28	15.14	6.14
10-20 Aug	23.4	14.75	8.65	34.6	20.2	44.6	26.7	13.02	19.82
20-31 Aug	42.4	18.58	32.47	19.5	16.6	47.5	30.83	14.24	36.41
1-10 Sep	0.26	12.89	19.84	5.9	11.3	42.1	4.1	19.02	21.49
10-20 Sep	0.07	7.77	12.14	3.9	8.5	37.5	5.29	9.33	17.45
20-30 Sep	0	5.62	6.52	0	5.2	32.3	0	3.41	14.04
1-10 Oct	0	4.37	2.15	0	3.4	28.9	0	2.77	11.27
10-20 Oct	0	0.81	1.34	0	2.9	26	0	4.06	7.21
20-31 Oct	0	0.32	1.02	0	2.5	23.5	0	1.98	5.23
1-10 Nov	0	0.28	0.74	0	1.4	22.1			
10-20 Nov	0	0.3	0.44	0	1.1	21			
20-30 Nov	0	0.29	0.15						

Water balance for 2013

The histogram below shows the variation over time of the water balance for the year 2013 (Fig. 14). Although the rainy season begins in July, this month is in deficit. Indeed, there is no effective rainfall. The evaporative demand from the atmosphere is very high with a strong decrease or even drying out of the soil's water supply. The first effective rains begin to occur from the first decade of August and reach their maximum at the end of this month with a height of 32.5 mm, it is the wettest month. The curve drops sharply in the first decade of September with a decrease of more than 10 mm in 10 days and then continues until it is cancelled at the end of the year. Despite the fact that in August we have a good and efficient water wave, the extremely arid climate of the area has not allowed us to increase the availability of water for recharge. Low rainfall with low intensities occurs during this year. As a result, there is a residual of 0.15 mm at the end of the season, i.e. a rate of 0.22% of annual rainfall. There is no longer enough water to supply the underground tanks. The year 2013 is less favourable to recharging.

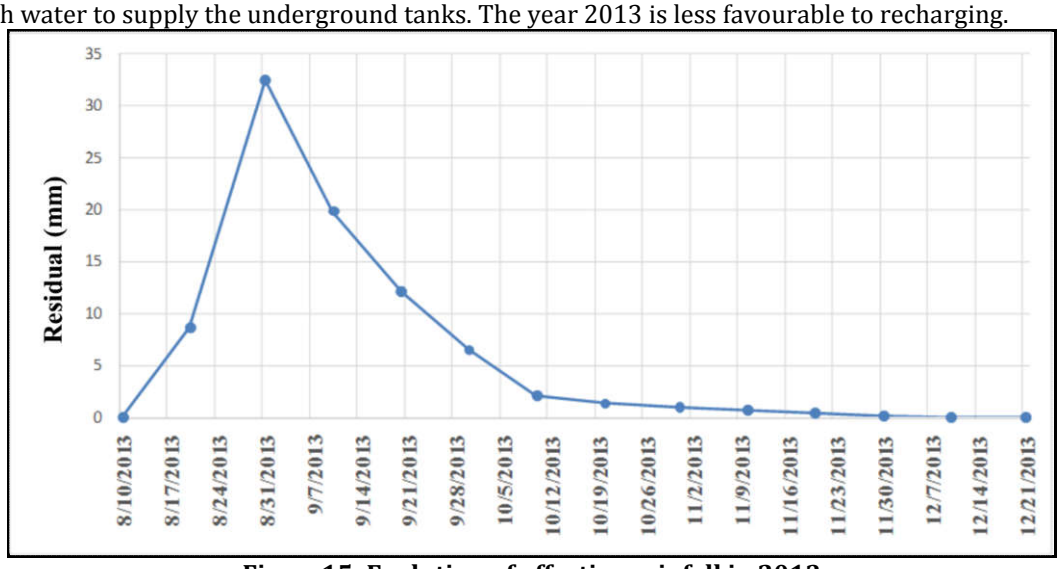

Figure15: Evolution of effective rainfall in 2013

Water balance for 2014

This year (2014) seems more favourable to recharging than the previous one (2013). The water balance records surpluses of more than 30 mm concentrated over the last twenty days of August and the first

twenty days of September (Fig. 16). After repeated rainfall events in August, residual rains increased significantly with a sharp 47.6 mm peak at the end of the month. After the last rains in September, evapotranspiration continues to reduce residual rainfall until all surface water disappears. The residual at the end of the season is 21 mm, or 17% of the annual rainfall.

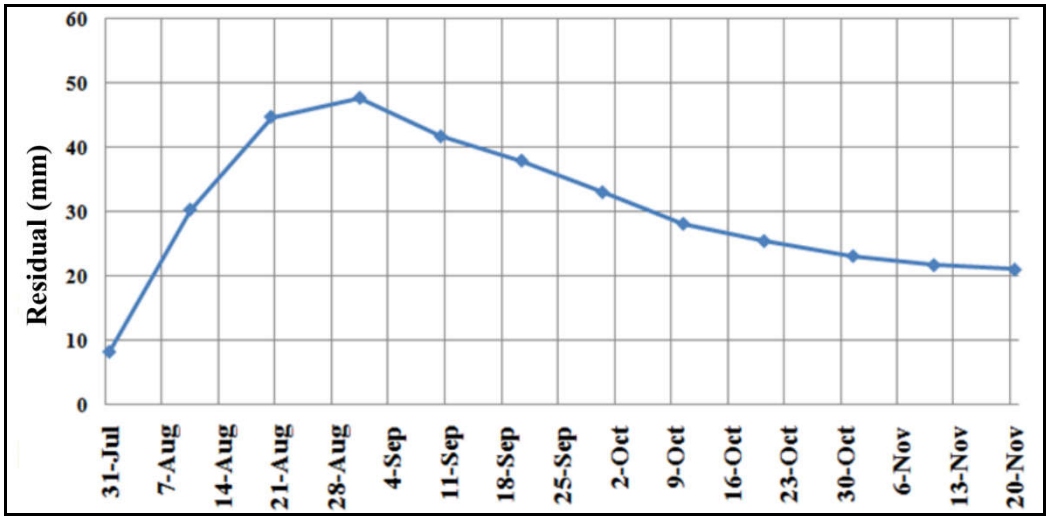

Figure16: Evolution of effective rainfall in 2014

Water balance for 2015

The water balance for 2015 is different from previous years. The effective water wave recorded at the beginning of the season is 6.1 mm and then gradually the maximum accumulation reaches 36.4 mm. The evaporation recovery causes the residual rains to drop, a 15 mm drop is recorded in less than ten days. This means that in this interval, there were no heavy rains with high intensities. At the end of the rainy season, after all surface water has disappeared, there is a residual of 5.23 mm (Fig. 26). The rate equivalent to this residual is 6% of the annual rainfall.

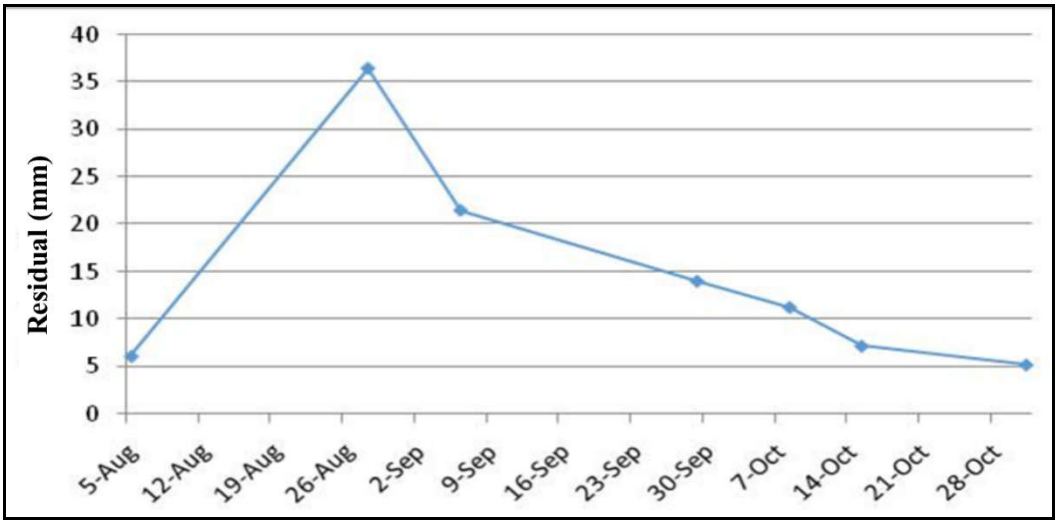

Figure17: Evolution of effective rainfall in 2015

DISCUSSION

Rainfall estimates from RFE2/FEWS-NET seem to be close to reality. Nevertheless, there are too many gaps in the field data to compare them with them. The analysis of rainfall variability shows a very high irregularity in the distribution of rainfall typical of a hyperarid environment. The influence of climate change in recent decades is believed to be one of the main causes [3]. The anomaly calculation indicates an upward trend marked by the recovery of good rainfall from 2010. This slight increase in rainfall does not reach the average of the years before 1970. This result is consistent with those found at the sub-regional level ([9]; [20]). This increase is also felt at the level of groundwater recharge, as confirmed by the results of GRACE and water balances.

The spatial distribution of precipitation shows a strong heterogeneity. As everywhere else in the country, there is a latitudinal evolution following a gradual and fairly regular decrease in precipitation [16]. The characterization of the four climatic zones would be due to the massif which constitutes a real climatic barrier to monsoon flows. This barrier curves the isohyets, placing the city of Fada, located at an altitude of about 570 m, and the city of Amdjarass, located at an altitude of about 830 m, on the same 80 mm isohyet. To the south of the massif, the area is arid and receives modest rains that rarely exceed 100 mm/year. Below this, the whole area is hyperarid and receives very low rainfall. The very high heat associated with disturbances in air mass circulation and other atmospheric parameters could be responsible for this distribution. And on the other hand it would be the latitudinal and topographical effects.

The results of the evapotranspiration estimation prove the effectiveness of the model. It seems to have worked well to estimate evapotranspiration from Landsat8 OLI/TIRS images for the Ennedi area and the entire northern part of the country. Because these arid areas have similar physical characteristics. We expected values less than 10 mm and this was the case. It should be noted that the model underestimates these values. This underestimation can be explained by uncertainties about intermediate variables entering the model such as albedo and surface temperature. Indeed, Landsat8 images are acquired in the morning around 9am, at which time the air temperature is low, which causes a decrease in the values of these two parameters. The accuracy of the model depends on the presence of water in the images, so the more water you have, the more accurate the estimate. However, at the end of July and in August, when almost all the rains fall, reasonable evapotranspiration values are observed. In the absence of water on the images, especially from September onwards, the model underestimates evapotranspiration. However, these estimated values should be considered with caution, as there is a lack of point field data measured on the ground to compare and validate them with satellite images. Similar studies have also shown the effectiveness of satellite images in estimating evapotranspiration [11];[7].

The method we used is at the scale of the catchment areas, but in these hyperarid areas the infiltration of water is very local and depends on the spatial and temporal variability of rainfall. If these constraints are taken into account, the effective rainfall could be higher than that calculated at the basin scale. The results of this study suggest that below a rainfall of 60 mm/year, effective rainfall is almost zero. However, there is a nuance that needs to be clarified, as recharging depends on the intensity and duration of the instant rainfall. This implies that this possible modern recharge could be explained by the fact that heavy rains with high intensities sometimes fall, leaving a sufficient quantity of water to escape evapotranspiration. The moisture accumulated during the summer and the geological structure of the region, consisting mainly of highly fractured primary sandstones and therefore having high porosity, facilitate water infiltration. Although there is a resumption of evaporation from the unsaturated zone, deep infiltration is not excluded because the groundwater level generally does not exceed 30 m at the southern edge of the massif. GRACE's results confirm these results. Because during the period 2013 - 2015, there is an increase in the potential for groundwater recharge.

As the variation in the piezometric level is at least partly dependent on the conditions of the recharge of the groundwater by rainwater, we can already make a correlation between them. The seasonal fluctuations in piezometry measured in 2013 and 2016 on the same structures argue in favour of direct seasonal recharge during the rainy season. The comparison concerns 26 structures, including 21 structures that capture the Paleozoic sandstone aquifer, 4 structures that capture alterations and fractures of the basement and only one structure that captures alluvial groundwater. The result shows that the piezometric level increased in 77% of cases, or 21 out of 26 structures (Fig. 18). In the rest of the structures, there was a decrease in the piezometric level (6 structures or 23%). The increase in water level varies from 0.12 to 4.39 m, with an average of 1.7 m. In general, these variations in groundwater level can be related to precipitation. Water level fluctuations, although not significant, prove that the water table receives a supply that renews water stocks.

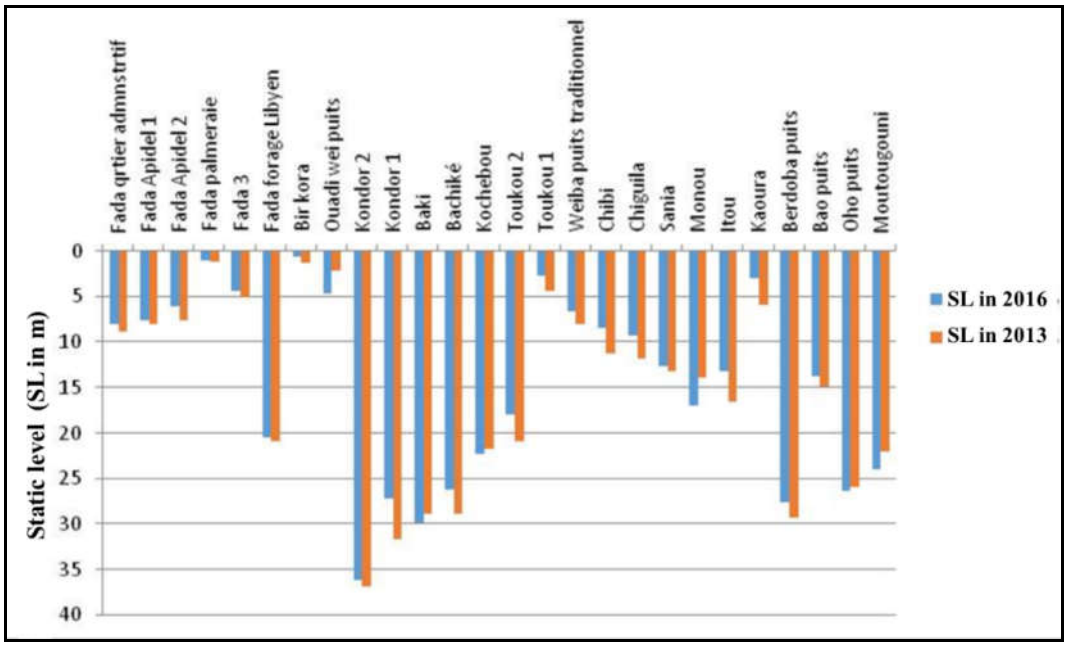

Figure18: Piezometric level fluctuations of wells

CONCLUSION

The results obtained in this study confirm the potential of satellite data to study climate variability and assess recharge in arid regions with low cloud cover. Despite the uncertainties associated with the different sources that have different spatial and temporal resolutions and despite the lack of ground data, the approach we used to estimate this uncertainty seems to be good for estimating a number of climate parameters. The advantage of these data is that they offer a good spatial distribution that is more precise and detailed than those in the field. The only disadvantage is that they have a very degraded temporal repetitiveness (10 days for FEWS-NET, 16 days for Landsat and about 1 month for GRACE), which hinders the quality of their monitoring.The study of climate variability shows that despite the exacerbated climatic conditions, the region is experiencing increased rainfall under the influence of the monsoon. However, the annual and monthly distribution is very heterogeneous. Deficit and surplus years appear with sometimes more than 100 mm of rainfall per year, which is rare in hyperarid areas. The annual average found in this series is 61 mm/year, well below that estimated before this period. The anomaly study identified two periods: a deficit period from 2000 to 2009 and a surplus period from 2010 to 2016. The cartographic representation of annual rainfall shows that the evolution of rainfall follows a southwest - northeast gradient. Isohyets evolve in curvature putting areas of different altitudes on the same level. The southern part of the massif records more rainfall at the expense of the northern slopes where the massif is a barrier to monsoon flows. Mapping of the two deficit and surplus periods shows that the last period is marked by a migration of isohyets towards the Northeast, which results in an increase in precipitation. Coupled with rainfall data, GRACE data show that the aquifer system is very sensitive to rainfall variations. Water storage varies according to rainfall. As the rainy season approaches, there is almost no variation, which proves our water balance hypothesis. The calculation of the water balance allowed us to understand that despite the intense evaporation activities, in a humid year, there will be a quantity of water that escapes and reaches the aquifers to feed the aquifers, sometimes sufficient to meet the needs of the population. This resource deserves to be well managed, because with the current climate change if years of drought are repeated, they will greatly weaken this resource. The S-SEBI model tested confirms the possibilities of solving the energy balance equation from LandSat8 OLI/TIRS images to estimate evapotranspiration in the northern part of the country, unlike theMODIS model tested by the ResEau project.

REFERENCES

1. Arino O. (1990). Surface albedo and short wavelength radiation balance: satellite contribution. Thesis Univ. Toulouse, INPT.
2. Bastiaanssen W.G.M, Ahmed M.D., Chemin Y. (2002). Satellite surveillance of evaporative depletion across the Indus Basin, Water Resource.Res. 38, pp. 1273-1282.
3. BURGEAP (2001). Pastoral hydraulics project in the B.E.T. Well sections and characteristics. End of project report, Ministry of the Environment and Water, 163p.

4. Da Silva B.B, Braga A.C, Braga C.C, De Oliveira L.M.M, Suzana M. G. L, Montenegro S.M.G.L, Junior B.B (2016). Procedures for calculation of the albedo with OLI-Landsat 8 images: Application to the Brazilian semi-arid. Res. Brasileira de Engenharia Agrícola e Ambiental, v.20, n ° 1, pp. 3-8.
5. Du C, Ren H, Qin Q, Meng J, Zhao S, (2015) .A practical split-window algorithm for estimating land Surface Temperature from Landsat 8 data. Remote Sens., Pp. 647-665.
6. FEWS-NET (2012). A climate trend analysis of Chad.Fact sheet 2012-3070.
7. Hamimed A, Nehal L, Khaldi A, Azaz H (2014). Contribution to the spatialization of the evapotranspiration of a semi-arid agro-system in Algeria through the use of remote sensing and the METRIC model. Physio-Geo, Volume 8.
8. Jérôme A.N, Yoboue K.B, N'daoule R (2015). Rainfall variability and its impact on water supply in rural areas in the department of Dimbokro (central-eastern Ivory Coast). European Scientific Journal, vol.11, No.35.
9. Mahé G (2006). Rain-flow variability in West and Central Africa in the 20th century: hydro-climatic changes, land use and hydrological modeling. Thesis Univ. Montpellier 2, 160p.
10. EH (2014). Hydrogeological map of the Republic of Chad at 1: 500,000. Sheet NE-34-SE Ennedi.
11. Olioso A, Jacob (2002). Estimation of evapotranspiration from remote sensing measurements. La Houille Blanche, n ° 1, pp. 62-67.
12. ORSTOM (1962). Study of surface hydrology in sub-desert and desert regions of black Africa. Study of the Ennedi massif and the northern region of Mortcha (Chad Basin). Land and water v. 38 pp. 46-73.
13. Parodi G.N, (2002). Algorithms and theory - Version 1.3, AHVRR Hydrological Analysis System. 77P.
14. Roche M (1960). Overview of the climate and hydrology of the Ennedi massif and the Mortcha plain. Saharan liaison bulletin n ° 37 pp. 41-51.
15. Roering G.J, Su Z, Menenti M (2000) .S-SEBI: A simple remote sensing algorithm to estimate the surface energy balance. Phy. Chem. Earth (B), vol. 25, n ° 2, pp. 147-157.
16. Schneider J.L (2001). Geological, archeology, hydrogeology. BRGM, vol. 1, 462p.
17. SDEA (2003). Water resources and the environment. HCNE-MEE-PNUD-DAES, 158p. Schneider J.L (2001). Geological, archeology, hydrogeology. BRGM, vol. 1, 462p.
18. IUCN (2016). Ennedi Massif: natural and cultural landscape (Chad). Evaluation report, ID 1475, pp. 105-113.
19. Wolf J.P (1964). Geological map of the Republic of Chad at 1: 1,500,000. BRGM.
20. Yao A.B, Goula B. T. A, Kouadio Z. A, Kouakou K. E, KANE A, Sambou S (2012). Analysis of climatic variability and quantification of water resources in the humid tropical zone: the case of the Lobo watershed in the west-west of the Ivory Coast. Rev. Isee. Sci. Technol., 19 (2012) 136 - 157.

CITE THIS ARTICLE

Miradj Habib Djafar, Abderamane Hamit and Marie-louise vogt. Climate variability and hydrogeological responses in the mountainous area of Ennedi (Chad) using remote sensing. Res. J. Chem. Env. Sci. Vol 7 [3] June 2019. 35-51